IEEE Photonics Journal
An IEEE Photonics Society Publication

Open Access

Transformation From Conventional Dissipative Solitons to Amplifier Similaritons in All-Normal Dispersion Mode-Locked Fiber Lasers

Volume 10, Number 1, February 2018

Yueqing Du
Xuewen Shu, ***Member, IEEE***

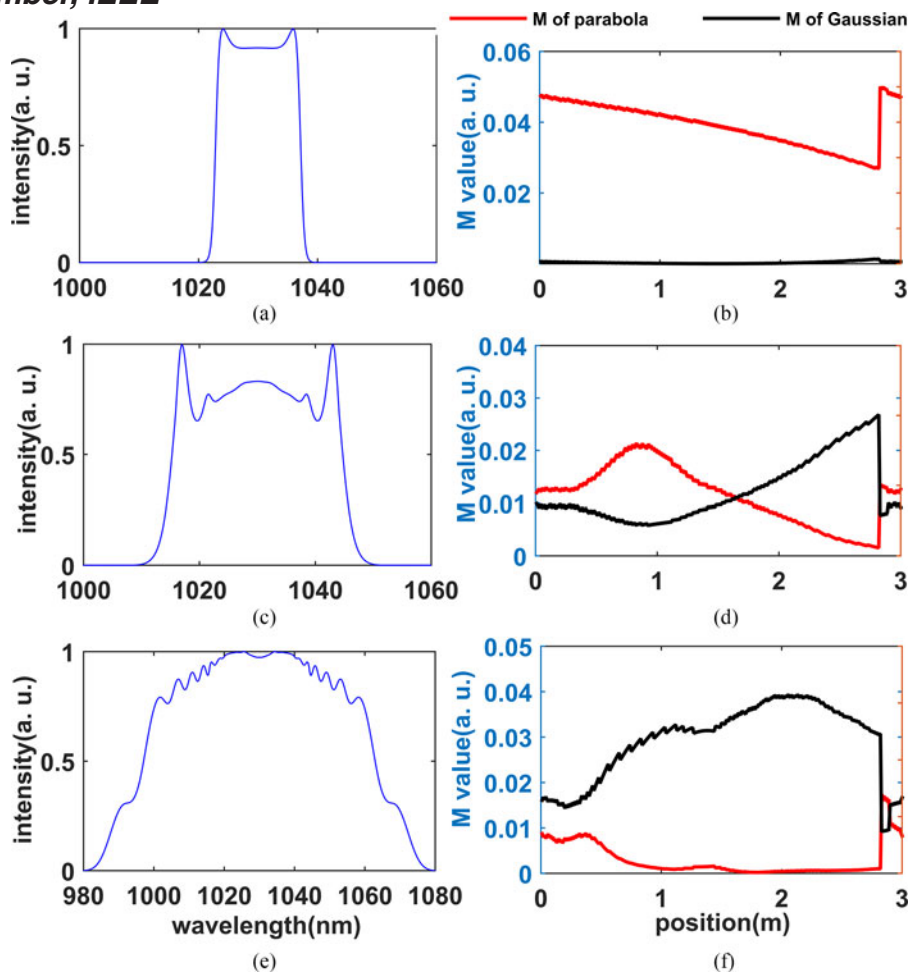

DOI: 10.1109/JPHOT.2018.2797942

IEEE photonics SOCIETY
IEEE

Transformation From Conventional Dissipative Solitons to Amplifier Similaritons in All-Normal Dispersion Mode-Locked Fiber Lasers

Yueqing Du and Xuewen Shu, *Member, IEEE*

Wuhan National Laboratory for Optoelectronics, School of Optical and Electronic Information, Huazhong University of Science and Technology, Wuhan 430074, China

DOI:10.1109/JPHOT.2018.2797942

Manuscript received November 8, 2017; revised January 15, 2018; accepted January 22, 2018. Date of publication January 25, 2018; date of current version February 7, 2018. This work was supported in part by the National Natural Science Foundation of China (61775074), in part by the National 1000 Young Talents Program, China, and in part by the 111 Project (B07038). Corresponding author: Xuewen Shu (e-mail: xshu@hust.edu.cn).

Abstract: We report the numerical demonstration of the transformation from dissipative solitons to amplifier similaritons in an all-normal dispersion ultrafast fiber laser for the first time. Different from the strong spectral filtering as well as large spectral and temporal breathing ratios for the typical amplifier similariton fiber lasers, our case has relatively weak spectral filtering and small spectral and temporal breath ratios ($<$6) for amplifier similaritons. An intermediate state between the dissipative soliton and amplifier similariton is discovered, which we call "dissipative similariton" considering its shaping mechanism and characteristics. Pulse regime dynamics is thoroughly explored. The chirp evolution together with pulse structures in time and frequency domains can be used to distinguish the three pulse regimes. This paper can enrich the pulse dynamics in all-normal dispersion fiber lasers and help one to properly design high-energy ultrafast laser configurations.

Index Terms: Fiber lasers, mode-locked lasers, solitons and polaritons.

1. Introduction

Passively mode-locked fiber lasers that work at net-normal and all-normal dispersion (ANDi) are very important candidates for high energy, ultrashort and broadband pulse generation [1]–[3], which can be used for high-intensity physics, frequency metrology, materials- processing and supercontinuum generation. Two kinds of ultrashort pulse in ANDi fiber lasers have been clearly demonstrated and well understood in the past ten years, one is dissipative soliton (DS) [4]–[6], the other is amplifier similariton (ASM) [7], [8]. The pulse shaping mechanism of the DS is based on composite balance between the normal dispersion, nonlinearity, gain and loss [1], [5], [9]. When the spectral filtering is offered by the limited gain bandwidth of the dope-fiber such as the erbium-doped fiber, the DS is also called the gain-guided soliton [10]. In fact, all the pulses generated in the non-adiabatic fiber lasers can be regard as a DS, however, the DS is usually used to represent those ultrashort pulses that are mainly shaped by the spectral filtering (SF) in the normal-dispersion mode-locked fiber lasers. The properties of the DS can be described through the averaged model of the complex Ginzburg-Landau equation (CGLE) [4], [5]. The ASM depends on the nonlinear attractor in the

fiber with normal-dispersion and distributed gain [11], [12], while a reverse process such as the SF is needed to satisfy the boundary conditions in the laser resonator [7], [12]. The pulse in the normal-dispersion fiber with distributed gain can reach the asymptotic state with a parabolic intensity profile and linearly positive chirp with enough distance ensured, which can be compressed to the transform-limited duration of 42 fs [13]. Flexible designs of the laser configuration can be used to generate ASM because the nonlinear attractor in the gain fiber is independent of the average cavity parameters [2], [14]. The most significant property of the ASM is wave-breaking-free under high pulse peak power because it can tolerate very strong nonlinear phase accumulation without wave-breaking, while the maximum energy and spectral width of the ASM is limited by the gain bandwidth of the gain fiber [15]–[19].

It seems that the configuration of the ANDi fiber lasers for ASM, usually including a segment of gain fiber with normal dispersion, a bandpass filter (BPF) and a saturable absorber (SA), is also capable of generating DS even the pulse shaping mechanisms of DS and ASM are quite different. There are many phenomenal characteristics for one to determine the regimes in normal-dispersion fiber lasers, such as the steep edges of the spectrum, M-shaped spectrum with side peaks and small spectral breathing ratio below 4 for the typical DSs [1]–[6] while the parabolic intensity profile, the spectrum with smooth edges and the large spectral breathing ratio more than 10 for the typical ASMs [8], [9], [12]–[15], [20]. One question is that- is there a transitional or intermediate state between the typical DS and ASM in the normal-dispersion ultrashort fiber laser? One kind of triangular shaped pulse has been observed in an dispersion-managed mode-locked fiber lasers in [21]. The authors in [21] find that the triangular pulse and the passive similariton can be switched through net-dispersion and gain parameters adjusting. The coexistent of the DS and ASM in an dispersion-managed mode-locked fiber laser has been demonstrated through nonlinear polarization evolution (NPE) experimentally [22] and theoretically [23]. The work in [23] finds that an ASM can be transformed into a DS when the pump strength is increased. The mechanism of such transformation is due to the strong filtering caused by the limited gain bandwidth when the pump strength is strong. One can note that the SF for ASM generation in [23] is offered by the distribute gain filtering of the EDF and the SA, which is different from the typical ANDi configuration with a lumped SF [2], [8], [12]–[17], [20]. As the common configuration of an ANDi fiber laser has a lumped SF, it is interesting to know whether the pulse regime transition can happen in the typical ANDi configuration because the ANDi fiber laser has become the dominant candidate for direct high-energy ultrashort pulse generation with simple configurations.

In this paper, we present a numerical demonstration of the transition from the DS to ASM in an ANDi ultrashort fiber laser with a lumped SF for the first time. We find that the transformation from the DS to ASM can be realized through the pump strength increasing in an ANDi ultrafast fiber laser with a lumped SF. The temporal and spectral breath ratios of the ASM in our simulations are about 4–6 and 4–5, respectively, which are quite different from the large ratios of the typical ASM in the ANDi fiber lasers. An intermediate state with the characteristics of both the DS and ASM is discovered and named “dissipative similariton” (DSM). Three kinds of pulse regimes can be clearly distinguished from their pulse structures and chirp evolution. By comparison with the previous work in [23], we find that the different cavity component managements can result in opposite pulse dynamics in an ANDi fiber laser. Our results can enrich the pulse dynamics in ANDi dissipative systems and help one to properly design high power ultrashort fiber lasers.

2. Model and Parameters in the Simulation

The model of the mode-locked ANDi fiber laser is schematically shown in Fig. 1. The main parts of the cavity are a segment of 2.8 m Yb-doped fiber (YDF), an 80:20 output coupler (OC), a lumped BPF, a segment of 0.2 m single-mode fiber (SMF) and a lumped saturable absorber (SA). The total length of the cavity is 3 m. We try to make the main part of the laser to be the gain fiber, which is also done in typical ASM fiber lasers [12]–[14]. If the SMF is too long, the similariton will gradually lose its self-similar property in the SMF and finally the similariton can’t be formed in the typical configuration of the similariton lasers (Gain fiber + SMF + SF + SA). Our simulation starts

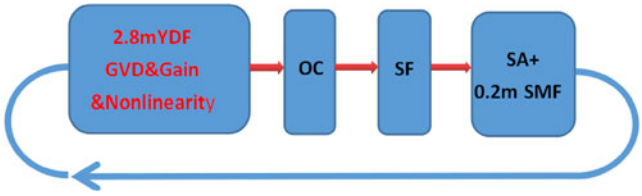

Fig. 1. Schematic of the fiber laser in our simulation.

from an arbitrary weak signal and the pulse runs from the YDF to SMF in each round. We use the extended Nonlinear Schrodinger Equation (NLSE) to describe the pulse propagating in the laser cavity:

$$\frac{\partial u}{\partial z} = -i\frac{\beta_2}{2}\frac{\partial^2 u}{\partial t^2} + i\gamma|u|^2 u + \frac{g}{2}u\left(1 + \frac{1}{\Omega^2}\frac{\partial^2}{\partial t^2}\right) \tag{1}$$

Where u is the envelope of the light pulse running in the fiber laser. β_2 is the second order dispersion, which is 23 ps^2/ km and 21 ps^2/ km in YDF and SMF, respectively. γ is nonlinear coefficient of the fiber, which is 4.7 $W^{-1}\,km^{-1}$ and 1.3 $W^{-1}\,km^{-1}$ in EDF and SMF, respectively. Ω represents the gain bandwidth of EDF and the full width at half maximum (FWHM) of the gain bandwidth is 40 nm in our simulation. g is the gain of the EDF, which is represented by:

$$g = g_0 \exp\left(-\int |u|^2 dt/Es\right) \tag{2}$$

Where Es is the saturable energy of the YDF, which also represents the pump strength. g_0 is the small signal gain of the YDF, which is 1.7 m^{-1} in our simulations. The transmission function of the amplitude of lumped SA is represented by:

$$T = \sqrt{1 - \alpha/(1 + P/P_0)} \tag{3}$$

Where α is the modulation depth of the SA, which has a value of 0.9. P is the instantaneous power of the light pulse. P_0 is the saturation power, which is 200 W in our simulations. The parameters of the SA can be generated through the flexible artificial SA through wave plates and PC controlling in the NPE mode-locked fiber lasers. The bandpass filter has a parabolic transmission function. We use the symmetric split-step Fourier method to implement our simulations. In the simulations, we choose different pump strengths Es and different bandwidths of the BPF while the rest of the parameters are fixed. The results can converge to the stable state in several hundred rounds in most cases, the presented results are the stable states at the round of 1000.

We use the misfit (M) value between the ultrashort pulse and its relative fitting curve to evaluate the pulse shape in the laser cavity [24]. The fitting curve has the same FWHM and peak power with those of the pulse intensity profile. The M value we use in this paper is calculated by:

$$M = \int \left[|u|^2 - |p|^2\right]^2 dt / \int |u|^4 dt \tag{4}$$

Where u is the normalized amplitude of the pulse, p is the normalized amplitude of the fitting shape (such as Gaussian, or square root parabola) with the same intensity FWHM of u^2. It is clear that larger M-value means the pulse shape deviates more from the fitting shape. We should note that stable solution of various shapes for the GLE can be realized through parameters adjusting [3]–[6], however, the typical intensity profile of the DS in our simulations is Gaussian, which is similar to the experiment results of a strong normal-dispersion DS fiber laser in [25]. In our simulations, the M values of the parabola and Gaussian are used to evaluate the relative shape of the ultrashort pulse.

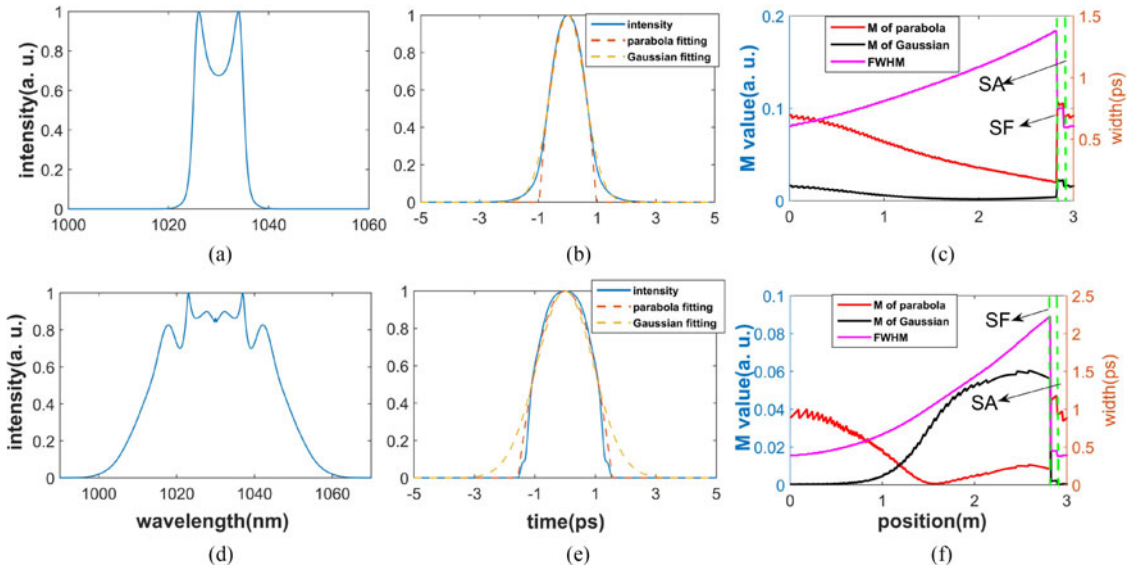

Fig. 2. Pulse characteristics under BPF bandwidth of 10 nm: (a) normalized spectrum of the pulse at the end of YDF with 0.4 nJ pump, (b) normalized intensity profile and fitting curves of the pulse at the end of YDF with 0.4 nJ pump, (c) M values of the parabola, Gaussian and FWHM evolution in the laser cavity with 0.4 nJ pump, (d) normalized spectrum of the pulse at the end of YDF with 5.2 nJ pump, (e) normalized intensity profile and fitting curves of the pulse at the end of YDF with 5.2 nJ pump, (f) M values of the parabola, Gaussian and FWHM evolution in the laser cavity with 5.2 nJ pump strength.

3. Results

3.1 From DS to ASM

We set the FWHM of the BPF to be 10 nm and the stable states of the mode-locked pulses under pump strengths of 0.4 nJ and 5.2 nJ are shown in Fig. 2. We can see from Fig. 2(a) that the spectrum at the pump strength of 0.4 nJ has steep edges and side peaks, which can be characterized as a typical DS. The pulse profile at the pump strength of 0.4 nJ has a Gaussian shape as seen in Fig. 2(b). The Gaussian shape fits better with the DS than the parabola. Pulse shape and width evolution under the pump strength of 0.4 nJ are shown in Fig. 2(c). We can get from Fig. 2(c) that the pulse keeps a Gaussian shape rather than the parabola because the M value of the parabola is larger than that of Gaussian in the laser cavity. Even the pulse doesn't reach the parabola in the cavity, it has an obvious tendency to evolve toward the parabola, which means the pulse shaping is also affected by the self-similar attractor in the gain fiber. The duration and spectral breathing ratios of the DS in the cavity are ∼2.31 and ∼1.13, respectively, which fall in the range of the DS breathing ratio [5]. From the results in Fig. 2(a)–(c), we can conclude that the pulse under the pump strength of 0.4 nJ is a typical DS. Pulse states become different when the pump strength reaches 5.2 nJ, which are shown in Fig. 2(d)–(f). As we can see from Fig. 2(d) that the spectrum has smooth edges compared with that in Fig. 2(a), which is the typical characteristic of an ASM. The oscillating structure in Fig. 2(d) can be explained by the difference between the chirp across the pulse and exact linearity [11]. The pulse hold a parabolic profile rather than the Gaussian shape in Fig. 2(e). One can get from Fig. 2(f) that the pulse quickly converges to the parabola within a distance of 1.5 m in the gain fiber and then keeps a relatively parabolic profile before the BPF. After the BPF, the ASM is reversed to a pulse with a Gaussian profile as seen in Fig. 2(f). The SA can decrease both the M values of the parabola and Gaussian. We can also obtain from the FWHM evolution that the ASM experiences much stronger breathing compared with the DS under the pump of 0.4 nJ. The temporal and spectral breathing ratios of the ASM are ∼5.85 and ∼4.41, respectively, which are much larger than that of the DS but smaller than that of a typical ASM. The relative small spectral breathing ratio in our case is due to the weak spectral filtering. Usually, the BPF bandwidth in the

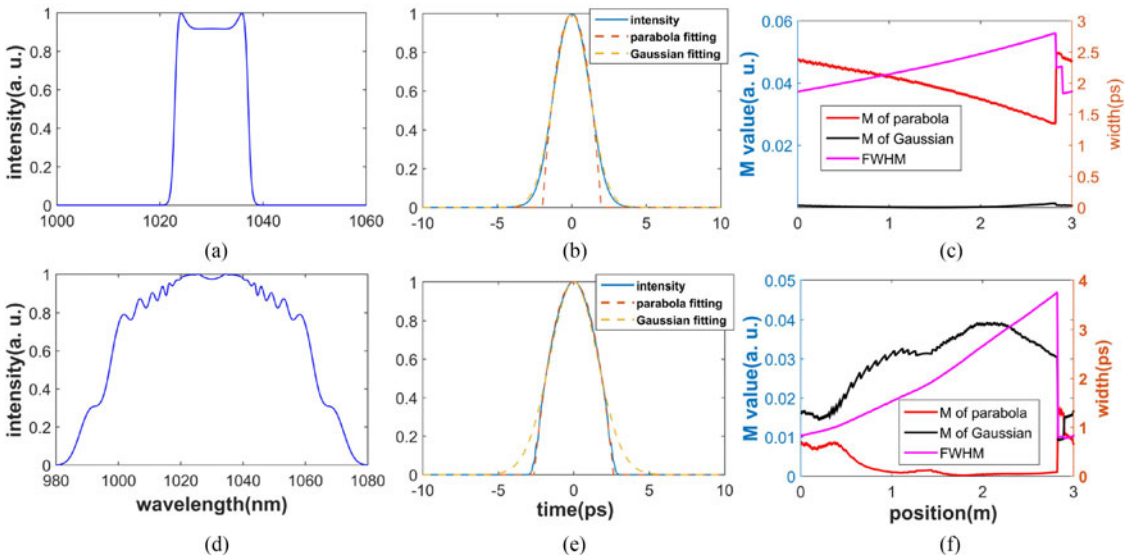

Fig. 3. Pulse characteristics under BPF bandwidth of 20 nm: (a) normalized spectrum of the pulse at the end of YDF with 1 nJ pump, (b) normalized intensity profile and fitting curves of the pulse at the end of YDF with 1 nJ pump, (c) M values of the parabola, Gaussian and FWHM evolution in the laser cavity with 1 nJ pump, (d) normalized spectrum of the pulse at the end of YDF with 20 nJ pump, (e) normalized intensity profile and fitting curves of the pulse at the end of TDF with 20 nJ pump, (f) M values of the parabola, Gaussian and FWHM evolution in the laser cavity with 20 nJ pump.

typical ASM fiber laser is ∼4 nm [12], which is strong to generate large spectral breathing ratio of more than 10. The evolution of the ultrashort pulse in Fig. 2(f) demonstrates the strong nonlinear attractor dominates the pulse shaping, so we can conclude that the ultrashort pulse under the pump strength of 5.4 nJ is an ASM rather than a DS considering both its pulse structure and evolution characteristics. From the results in Fig. 2, it comes out that both the DS and ASM can exist in the same laser system with only the pump strength adjusting.

To verify the transition from a DS to an ASM is not a unique phenomenon under specific parameters, we set the BPF width to be 20 nm and observe the pulse characteristics under different pump strengths. The spectrum of the pulse at the end of YDF with 1 nJ pump strength is shown in Fig. 3(a). We can see from Fig. 3(a) that it has an M-shaped profile with side peaks and steep edges, which are typical characteristics of a DS. The pulse holds a Gaussian profile rather than the parabola as one can see from Fig. 3(b). The shape evolution under the pump strength of 1 nJ in Fig. 3(c) shows that the DS keeps a Gaussian profile in the cavity. The DS has a small duration breathing in the cavity as shown in Fig. 3(c). The temporal and spectral breath ratios are ∼1.52 and ∼1.05, respectively, which are the typical values of a DS in ANDi fiber lasers. Clearly, a DS is formed when the pump strength is 1 nJ under BPF width of 20 nm. Pulse characteristics under a pump of 20 nJ are shown in Fig. 3(d)–(f). The spectrum at the end of YDF in the cavity is shown in Fig. 3(d). We can see from Fig. 3(d) that the spectrum has a much more complex structure and smoother edges compared with those of the DS. Such a kind of spectrum can be observed in many previously experimental and numerical results of the ASM [14]–[19]. The bandwidth of the spectrum in Fig. 3(d) is 66 nm. We can get from Fig. 3(e) that the pulse has a parabolic profile, which is the characteristic of an ASM. The pulse keeps a parabolic profile in the cavity as shown in Fig. 3(f), which demonstrates the dominant effect of the nonlinear attractor in the gain fiber. The pulse experiences larger duration breathing in Fig. 3(f) compared with Fig. 3(c). The temporal and spectral breath ratios are ∼4.88 and ∼4.14, respectively, which are of the similar magnitude to the ASM in Fig. 2. In a word, the simulation results in Fig. 3 demonstrate that the ultrashort pulse can transform from a DS to an ASM with the pump strength increasing from 1 nJ to 20 nJ under BPF bandwidth of 20 nm.

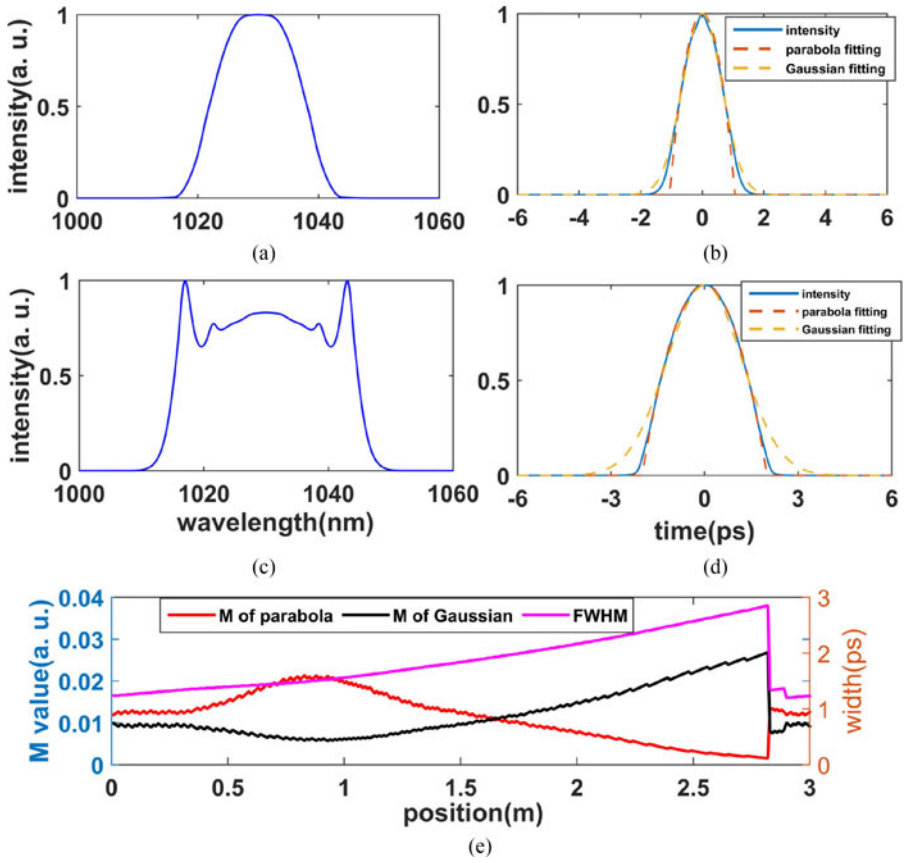

Fig. 4. Pulse characteristics under pump strength of 3 nJ with BPF bandwidth of 20 nm: (a) pulse spectrum at the 0.88 m, (b) pulse intensity profile and its fitting curves at 0.88 m, (c) pulse spectrum at 2.8 m, (d) pulse intensity profile and its fitting curves at 2.8 m, (e) pulse evolution in the cavity.

3.2 Intermediate DSM Between DS and ASM

In Section 3.1, we have demonstrated the formation of DS and ASM in the same cavity with the pump strength adjusting. The case in Section 3.1 are typical DSs and ASMs with clear characteristics. We will reveal an intermediate state between the DS and ASM in this section. We set the pump strength to be 3 nJ under the same BPF bandwidth of 20 nm as the case of Fig. 3. The results are shown in Fig. 4. We can see from Fig. 4(a) that the pulse at 0.88 m has smooth edges like the ASM while the flat top of the spectrum is different from the ASM. The profile of the pulse at 0.88 m in Fig. 4(b) shows neither parabola nor Gaussian shape, however, it is much nearer to the Gaussian. Things become different at 2.8 m as shown in Fig. 4(c) and (d), the pulse is parabolic in time domain like the ASM while has a M-shape spectrum with steep edges like the DS in frequency domain. It is not suitable for us to evaluate the pulse in Fig. 4(a) or (c) as a DS or an ASM because the pulse has both characteristics of the DS and ASM. The M value evolution in Fig. 4(e) shows that the pulse holds an intermediate shape between parabola and Gaussian from 0–1.65 m in the gain fiber and gradually converges to a parabola at the end of the YDF. The shape evolution in this case is quite different from an ASM. For an ASM, the shape of the ultrashort pulse quickly converges to the parabola from the beginning of the YDF as shown in Figs. 2(f) and 3(f), while in Fig. 4(c), the pulse holds an unclear tendency of the shape evolution from 0–0.88 m while gradually converges to the parabola from 0.88 m–2.8 m. It is clear that the self-similar nonlinear attractor does not dominate the pulse shaping from 0–0.88 m. The temporal and spectral breathing ratios of the pulse are ∼2.37 and ∼2.01, respectively, which are smaller than the typical ratio of an ASM. We call such a pulse state “dissipative similariton”.

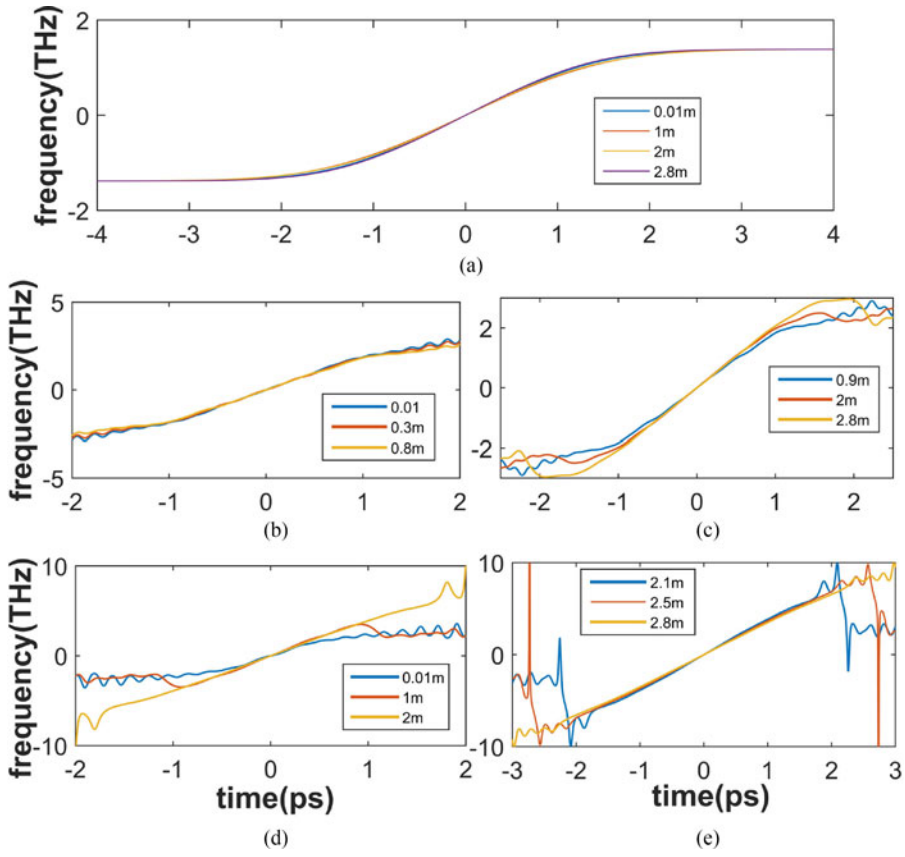

Fig. 5. Pulse's chirp evolution and regimes under different pump strengths when the bandwidth of BPF is 20 nm: (a) 1 nJ, DS, (b) 3 nJ, DSM from 0.01 m–0.8 m, (c) 3 nJ, DSM from 0.9 m–2.8 m, (d) 20 nJ, ASM from 0 ∼ 2 m, (e) 20 nJ, ASM from 2 m ∼ 2.8 m.

3.3 Chirp Evolution of the DS, DSM and ASM

To give an insight into the difference between the DS, DSM and ASM, we research the chirp evolution of three different pulse states under pump strengths of 1 nJ, 3 nJ and 20 nJ with SF bandwidth of 20 nm, respectively. The chirp is represented by the instantaneous frequency across the pulse. The results are shown in Fig. 5. Fig. 5(a) shows the chirp evolution of the DS under a pump strength of 1 nJ. We can see from Fig. 5(a) that the chirp of the DS is positive and nonlinear across the pulse. The chirp has no obvious alternation and keeps a stable state in the laser cavity. The chirp evolution of the DSM in Fig. 5(b) and (c) shows two distinct stages. One is the evolution from 0 ∼ 0.88 m in Fig. 5(b), where the chirp keeps a nonlinear positive state similar to the case of the DS in Fig. 5(a), the other is the evolution from 0.88 m–2.8 m in Fig. 5(c), where the nonlinear chirp is shaped into the linear chirp at the end of the YDF. This phenomenon is in accordance with the two stages of the pulse shape evolution in Fig. 4(e), where the shape of the pulse gradually converges to the parabola after 0.88 m. The linear shaping of the chirp and the parabolic shaping of the intensity profile are the evidences of the nonlinear self-similar attractor of ASM at the second stage (from 0.88 m–2.8 m) in Figs. 4(e) and 5(c). The nonlinear attractor in this intermediate case is not strong enough to shaping the pulse into the absolute ASM in the limited length of the gain fiber, which results in the DSM generation with both characteristics of the DS and ASM. The ASM under a pump strength of 20 nJ also has two distinct chirp evolution stages as shown in Fig. 5(d) and (e). The first stage is shown in Fig. 5(d), where one can see that the chirp is nonlinear positive and gradually shaping into the linear positive chirp from 0 m to 2 m, which demonstrates the nonlinear attractor has strong effect in this stage. After the chirp becomes linear, the slope of the instantaneous frequency across the

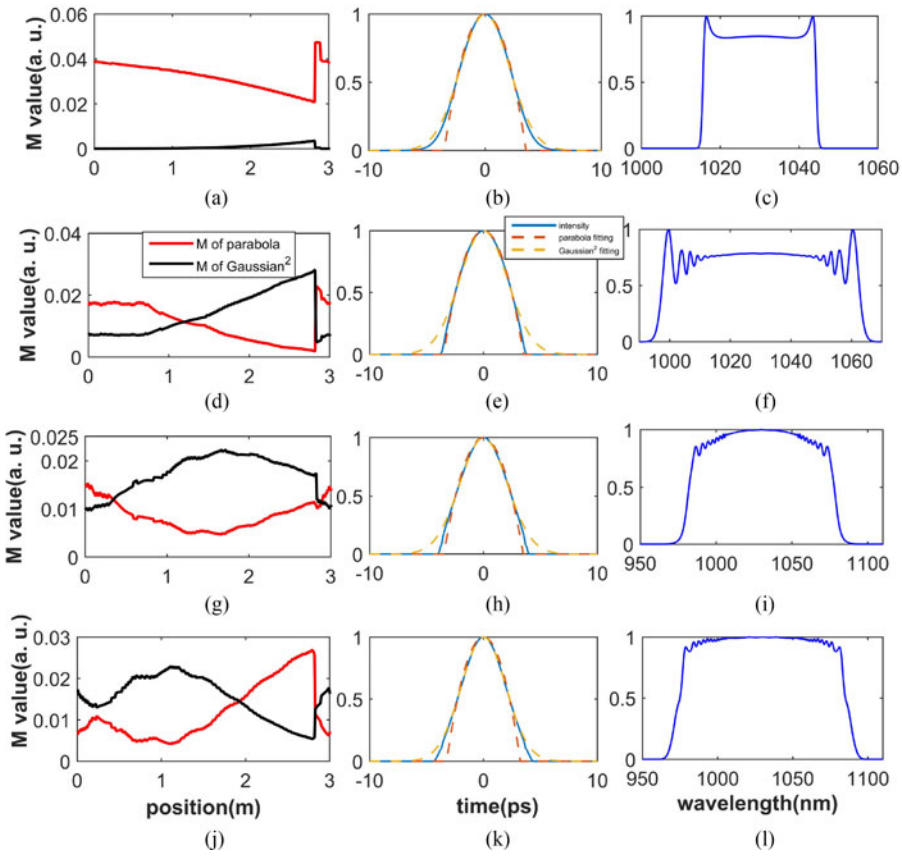

Fig. 6. Pulse characteristics under different pump strengths when the BPF bandwidth is 35 nm, (a)–(c): 5 nJ pump strength, (d)–(f): 20 nJ pump strength, (g)–(i): 50 nJ pump strength, (j)–(l): 100 nJ pump strength. Middle and right columns are the pulse intensity profiles and spectra at the end of YDF under different pump strengths.

pulse decreases slightly from 2 m to 2.8 m as shown in Fig. 5(e). The decreasing of the chirp is caused by the saturation of the gain. The gain provided by the YDF decreases as the pulse energy increasing in the gain fiber, which results in the decreasing of the chirp of the ASM [11]. In a word, the three regimes of ultrashort in this ANDi fiber laser have very distinct chirp evolution in the laser cavity.

3.4 Weak Lumped Spectral Filtering

We have checked that with the BPF bandwidth ranging from 10 nm to 32 nm, the pulse regime transition experiences the above three steps with the pump strength increasing, namely, DS, DSM and ASM. The DS will break into multi-pulses at high pump strength when the BPF bandwidth is smaller than 10 nm, which is caused by the strong spectral loss of the BPF when the DS has wide spectrum at high pump strength. We note that the experimental results of the dissipative soliton resonance (DSR) in [26] also have similar behavior. The DS will break into multi-pulses when the pump strength is high enough, however, DSR can be obtained at high pump strength with polarization controller (PC) adjusting [26]. We estimate that the PC adjusting in [26] can result in the changing of bandwidth of the artificial birefringent filter, which can make the laser compatible with the high-energy DSR generation at high pump strength. When the BPF bandwidth is wider than 32 nm in our simulations, four steps will happen, namely DS, DSM, ASM and DSM again. We set the bandwidth of the BPF to be 35 nm, the pulse characteristics under different pump strengths are shown in Fig. 6. Fig. 6(a)–(c) are the DS under a pump strength of 5 nJ. The rectangular

M shaped spectrum together with the Gaussian intensity profile indicate the DS formation in the cavity. Fig. 6(d)–(f) are the pulse characteristics under a pump strength of 20 nJ, which have the characteristics of the DSM formation in the cavity similar to the case of Fig. 4. Fig. 6(g)–(i) are the pulse characteristics under a pump strength of 50 nJ. We can see from Fig. 6(g) that the pulse keeps a parabolic profile in the laser cavity. The profile in Fig. 6(h) demonstrates the parabolic profile of the pulse at the end of the YDF, however, the pulse shape deviates from the parabola to some extent, which is caused by the disturbing of the gain filtering. The gain filtering is not strong enough to destroy the self-similar evolution in the YDF but can affect the self-similar evolution in the gain fiber. The spectrum of the ASM in Fig. 6(i) has smooth edges and a structural top, which is different from the M shaped spectrum of the DS. When we increase the pump strength to 100 nJ, the pulse regime becomes DSM again. As we can get from Fig. 6(j) that the pulse keeps a parabola from 0–1 m in the YDF and gradually moves toward the Gaussian shape after 1 m. The pulse at the end of YDF has a Gaussian shape as shown in Fig. 6(k). The spectrum has a near rectangular shape with steep edges and a flat top as the DS, which means the pulse shaping is strongly affected by the gain filtering. The DSM formation with 100 nJ pump strength is caused by the gain filtering of the YDF. The pulse has a narrow spectrum from 0–1 m and the gain filtering has weak impact on the self-similar evolution. When the bandwidth of the spectrum increases, because of the self-similar evolution, the gain filtering has a strong impact on the pulse-shaping in the cavity and the pulse has much more characteristics of the DS due to the dissipative process in the gain fiber. We also increase the pump strength to a much larger value to check whether the pure DS can be formed in the cavity, no DS emerges but the noise-like pulse generates. We can note that the DSMs in Fig. 6(d) and (j) have opposite shape evolution in the cavity. The DSM under the pump strength of 20 nJ moves from the DS toward the ASM in the cavity while the DSM under the pump strength of 100 nJ moves from the ASM toward the DS in the cavity.

4. Discussion

In our case, DS happens at lower pump strength while ASM is at higher pump strength. The lumped SF offered by the BPF facilitates the formation of the DS under low pump strength while the strong nonlinear attractor facilitates the formation of the ASM under high pump strength. In our simulation of this ANDi ultrafast fiber laser, we find that the breathing ratios of the ASM in temporal and spectral domains are smaller than the typical values in ANDi ASM fiber lasers. The essential difference between the DS and ASM is whether there exists the nonlinear attractor of the gain fiber, namely the pulse reaches the asymptotic solution in the gain fiber with normal dispersion or the fiber with decreasing dispersion [14]. When the nonlinear attractor is weak, it is obvious that the pulse is DS and its evolution depends on the composite balance between the normal dispersion, nonlinearity, gain and spectral filtering. When the nonlinear attractor is strong, the pulse reaches the asymptotic solution and keeps the evolution of the similariton, we call such a pulse ASM because its shaping mechanism is dominated by the nonlinear attractor even the dissipative process also plays an assistant role for the self-consistent evolution. When the nonlinear attractor and dissipative process both dominate the pulse shaping, we call the pulse DSM. In [20], the pulse holds the characteristics of both the DS and ASM, the nonlinear attractor induces the pulse to evolve towards the ASM while a 30-nm BPF is used as a dissipative component to stabilize the pulse evolution. The nonlinear attractor is not dominant due to the limited length of the gain fiber. The pulse has the characteristics of both the ASM (large spectral breathing ratio of $\sim$40) and DS (steep edges of the spectrum). We speculate that the ultrashort pulse in [20] can be regard as a DSM due to the composite balance between the nonlinear attractor in the gain fiber and the dissipation of the SF.

Different pulse shaping mechanisms are accompanied with different characteristics. The coexistence of the different mechanisms should be pervasive in different configurations as long as there exists a gain fiber with normal-dispersion as a trigger for the nonlinear attractor. One can adjust the cavity parameters to choose the dominant mechanism of the pulse shaping. We can conclude from our simulation results that to obtain the amplifier similariton, long gain fiber, strong pump strength and weak spectral filtering are preferred during experimental realization. Long gain fiber

and strong pump strength ensure sell-similar evolution while weak spectral filtering avoids the pulse breaking before the pulse changes into the ASM with high pump strength. We can note that the two attractors of the traditional soliton in anomalous-dispersion and the ASM in normal-dispersion can simultaneously exist in the dispersion-managed fiber lasers in [7], [18], which is different from the transformation from the DS to ASM at different pump strengths in our case. The soliton-shaping and ASM-shaping happen simultaneously at different parts of the lasers in [7], [18] with proper parameters management. However, the ASM-shaping (nonlinear attractor) and part of the DS-shaping (gain and balance between the nonlinearity and normal-dispersion) happen simultaneously in the same part (gain fiber with normal-dispersion) in our laser, so it is not easy or possible to observe the simultaneous happening of the DS and ASM in different parts of the ANDi fiber laser due to the competition between the dissipation and self-similar attractor. In our simulations, we use the CGLE to describe the soliton propagation, which demonstrates the transformation from conventional DS to ASM is independent of the polarization properties. However, one should note that polarization is an important freedom of the soliton and the coupled CGLEs can give a more accurate simulation of the vector solitons. High-order vector soliton [27], vector DSs [28] and vector ASMs [29] have been experimentally demonstrated, which manifest themselves with very interesting polarization dynamics. We think that with polarization taken into consideration, one can find many useful and interesting results of the transformation from DS to ASM.

5. Conclusion

We have explicitly demonstrated the transformation from the DS to ASM in an ANDi mode-locked fiber laser with a lumped SF for the first time. The DSM concept is proposed in our paper to describe the intermediate state between the typical DS and typical ASM, which has both characteristics of the DS and ASM. DS, DSM and ASM can be gradually formed through the pump strength increasing with the rest cavity parameters being fixed when the lumped SF is within the range of 10–32 nm. When the BPF bandwidth is larger than 32 nm, the distribute gain filtering in YDF can also result in DSM formation when the pump strength is strong. The chirp evolution in the laser cavity can be used to clearly distinguish the three different pulse regimes. The chirp evolution of the DS keeps a nonlinear state during the propagation in the cavity. The chirp of the DSM evolves with the nonlinear state at the initial stage and then moves towards the linear positive chirp driven by the nonlinear attractor in rest of the gain fiber, which means the nonlinear attractor is not strong enough in the regime of DSM. As for the ASM, the nonlinear chirp evolves into a linear chirp in a distance of 2 m due to the nonlinear attractor and then the linear chirp decreases with the distance as a result of the gain saturation. Clear chirp evolution together with the temporal and spectral structures clarify the pulses in the ANDi laser into the three different regimes. Our simulation results enrich the pulse dynamics of the ANDi dissipative laser systems and can help one to choose proper laser parameters in experiments.

References

[1] F. W. Wise, A. Chongm, and W. H. Renninger, “High-energy femtosecond fiber lasers based on propagation at normal dispersion,” *Laser Photon. Rev.*, vol. 2, no. 1–2, pp. 58–73, Feb. 2008.
[2] A. Chong, L. G. Wright, and F. W. Wise, “Ultrafast fiber lasers based on self-similar pulse evolution: a review of current progress,” *Rep. Prog. Phys.*, vol. 78, Oct. 2015, Art. no. 113901.
[3] X. M. Liu, “Pulse evolution without wave-breaking in a strongly dissipative-dispersive laser system,” *Phys. Rev. A*, vol. 81, no. 5, May 2010, Art. no. 053819.
[4] P. Grelu and N. Akhmediev, “Dissipative solitons for mode-locked lasers,” *Nature Photon.*, vol. 6, pp. 84–92, Feb. 2012.
[5] W. H. Renninger, A. Chong, and F. W. Wise, “Dissipative solitons in normal-dispersion fiber lasers,” *Phys. Rev. A*, vol. 77, no. 2, Feb. 2008, Art. no. 023814.
[6] A. Chong, W. H. Renninger, and F. W. Wise, “Properties of normal dispersion femtosecond fiber lasers,” *J. Opt. Soc. Amer. B*, vol. 25, no. 2, pp. 140–148, Feb. 2008.
[7] B. Oktem, C. Ulgudur, and F. O. ILday, “Soliton-similariton fiber laser,” *Nature Photon.*, vol. 4, pp. 307–311, Mar. 2010.
[8] W. H. Renninger, A. Chong, and F. W. Wise, “Self-similar pulse evolution in an all-normal dispersion laser,” *Phys. Rev. A*, vol. 82, no. 2, Aug. 2010, Art. no. 021805.

[9] W. H. Reninger, A. Chong, and F. W. Wise, Pulse shaping and evolution in normal dispersion mode-locked fiber lasers," *IEEE J. Sel. Topic Quantum Electron.*, vol. 18, no. 1, pp. 389–398, Jan./Feb. 2012.
[10] L. M. Zhao, D. Y. Tang, and J. Wu, "Gain-guided soliton in a positive group-dispersion fiber laser," *Opt. Lett.*, vol. 31, no. 12, pp. 1788–1790, Jun. 2006.
[11] V. I. Kruglov, A. C. Peacock, and J. D. Harvey, "Self-similar propagation of parabolic pulses in normal-dispersion fiber amplifiers," *J. Opt. Soc. Amer. B*, vol. 19, no. 3, pp. 461–469, Mar. 2002.
[12] B. G. Bale and S. Wabnitz, "Strong spectral filtering for a mode-locked similariton fiber laser," *Opt. Lett.*, vol. 35, no. 14, pp. 2466–2468, Jul. 2010.
[13] B. Nie, D. Pestov, F. W. Wise, and M. Dantus, "Generation of 42-fs, and 10-nJ pulses from a fiber laser with self-similar evolution in the gain segment," *Opt. Exp*, vol. 19, no. 13, pp. 12074–12080, Jun. 2011.
[14] Y. X. Tang, Z. W. Liu, W. Fu, and F. W. Wise, "Self-similar pulse evolution in a fiber laser with a comb-like dispersion-decreasing fiber," *Opt. Lett.*, vol. 41, no. 10, pp. 2290–2293, May 2016.
[15] A. Chong *et al.*, "Pulse generation without gain-bandwidth limitation in a laser with self-similar evolution," *Opt. Exp*, vol. 20, no. 13, pp. 14213–14220, Jun. 2012.
[16] C. Aguergaray, D. Mechin, V. Kruglov, and J. D. Harvey, "Experimental realization of a mode-locked parabolic Raman fiber oscillator," *Opt. Exp*, vol. 18, no. 8, pp. 8680–8687, Apr. 2010.
[17] V. I. Kruglov, C. Aguegaray, and J. D. Harvey, "Parabolic and hyper-Gaussian similaritons in fiber amplifiers and lasers with gain saturation," *Opt. Exp*, vol. 20, no. 8, pp. 8741–8754, Apr. 2012.
[18] Z. X. Zhang, B. Oktem, and F. O. ILday, "All-fiber-integrated soliton-similariton laser with in-line fiber filter," *Opt. Lett.*, vol. 37, no. 17, pp. 3489–3491, Sep. 2012.
[19] H. Liu, Z. W. Liu, E. S. Lamb, and F. W. Wise, "Self-similar erbium-doped fiber laser with large normal dispersion," *Opt. Lett.*, vol. 39, no. 4, pp. 1019–1021, Feb. 2014.
[20] Y. Lan, Y. J. Song, M. L. Hu, B. W. Liu, L. Chai, and C. Y. Wang, "Enhanced spectral breathing for sub-25 fs pulse generation in a Yb-fiber laser," *Opt. Lett.*, vol. 38, no. 8, pp. 1292–1294, Apr. 2013.
[21] S. Boscolo and S. K. Turitsyn, "Intermediate asymptotics in nonlinear optical systems," *Phys. Rev. A*, vol. 85, no. 4, Apr. 2012, Art. no. 043811.
[22] J. S. Peng, L. Zhan, Z. C. Gu, K. Qian, S. Y. Luo, and Q. S. Shen, "Experimental observation of different pulse solutions of the Ginzburg-Landau equation in a mode-locked fiber laser," *Phys. Rev. A*, vol. 86, no. 3, Sep. 2012, Art. no. 033808.
[23] J. S. Peng, "Gain dependent pulse regimes transition in a dissipative dispersion-managed fiber laser," *Opt. Exp*, vol. 24, no. 3, pp. 3046–3054, Feb. 2016.
[24] C. Finot, F. Parmigiani, P. Petropoulos, and D. J. Richardson, "Parabolic pulse evolution in normally dispersive fiber amplifiers preceding the similariton formation regime," *Opt. Exp*, vol. 14, no. 8, pp. 3161–3170, Apr. 2006.
[25] A. Cabbase, B. Ortac, G. Martel, A. Hideur, and J. Limpert, "Dissipative solitons in a passively mode-locked Er-doped fiber with strong normal dispersion," *Opt. Exp*, vol. 16, no. 23, pp. 19322–19329, Nov. 2008.
[26] X. Wu, D. Y. Tang, H. Zhang, and L. M. Zhao, "Dissipative soliton resonance in an all-normal-dispersion erbium-doped fiber laser," *Opt. Exp*, vol. 17, no. 7, pp. 5580–5584, Mar. 2009.
[27] D. Y. Tang, H. Zhang, L. M. Zhao, and W. Xu, "Observation of high-order polarization-locked vector solitons in a fiber laser," *Phys. Rev. Lett.*, vol. 101, no. 15, Oct. 2008, Art. no. 153904.
[28] H. Zhang, D. Y. Tang, L. M. Zhao, X. Wu, and H. Y. Tam, "Dissipative vector solitons in a dispersion-managed cavity fiber laser with net positive cavity dispersion," *Opt. Exp*, vol. 17, no. 2, pp. 455–460, Jan. 2009.
[29] M. Olivier and M. Piche, "Vector similariton erbium-doped all-fiber laser generating sub-100-fs nJ pulses at 100 MHz," *Opt. Exp*, vol. 24, no. 3, pp. 2336–2350, Jan. 2016.